Struct Chem (2011) 22:77–87
DOI 10.1007/s11224-010-9686-7

ORIGINAL RESEARCH

# X-ray studies, spectroscopic characterisation and DFT calculations for Mn(II), Ni(II) and Cu(II) complexes with 5,6-diphenyl-3-(2-pyridyl)-1,2,4-triazine

**J. G. Małecki · B. Machura · A. Świtlicka**

Received: 9 September 2010 / Accepted: 3 November 2010 / Published online: 26 November 2010


**Abstract** New complexes with formula $[M(SCN)_2(L)_2]$ where M = Mn(II), Cu(II) were synthesized in simple reactions of metal chlorides with ammonia thiocyanate and 5,6-diphenyl-3-(2-pyridyl)-1,2,4-triazine (pytz) ligand in methanol solutions. In the reaction of $NiCl_2{\cdot}6H_2O$ and pytz ligand the $[NiCl_2(pytz)_2]{\cdot}2CH_3OH$ complex was obtained. The complexes were studied by IR, UV–vis, EPR spectroscopy and X-ray crystallography. Electronic structures of the complexes were calculated using DFT method, and apart from the descriptions of frontier molecular orbitals and the relocation of the electron density of the compounds, the bonding properties in the complexes were determined.

**Keywords** Manganese(II) · Copper(II) · Nickel(II) complexes · 5,6-Diphenyl-3-(2-pyridyl)-1,2,4-triazine · X-ray structure · UV–vis · DFT · EPR

## Introduction

Numerous compounds containing the 1,2,4–triazine moieties are well known in natural materials and show interesting biological, pharmacological and medicinal properties. 4-Amino-5-oxo-3-phenylamino-1,2,4-triazine has a powerful inhibiting effect on the cell wall lignification catalysed by peroxidases, and alters the integrity of chloroplast. Some of the 3,5,6-trisubstituted-1,2,4-triazines can be active as blood platelet aggregation inhibitors and others exhibit antiviral inhibitory activity (against influenza viruses for example), significant activity towards leukaemia and ovarian cancer, and anti-HIV activity [1]. More recently, it has been revealed that a zinc–dppt complex (dppt = 5,6-diphenyl-3-(2-pyridyl)-1,2,4-triazine) associated to a biocide could have significant biocidal effects on living cells including those of microorganisms (bacteria and fungi), cell culture system, plants and animals [2]. Another interesting property of the derivatives of 1,2,4-triazine compounds is formation of coloured complexes when they are coordinated to a metal ion. In particularly, the ligand 5,6-diphenyl-3-(2-pyridyl)-1,2,4-triazine has been widely used as an sensitive reagent for the determination of Fe(II) by spectrophotometric methods, in natural and waste waters [3, 4].

On the other hand, investigations on the syntheses, crystal, molecular and electronic structures of metal complexes containing ambidentate ligands are of great interest in connection with the accumulation of metal complexes having ambidentate ligands and with regulation the reactivities of active sites on metal complexes. Many transition metal complexes containing ambidentate ligands have been synthesized, and their structures, physical properties and linkage isomerization reactions of ambidentate units have been investigated. Among the ambidendate ligands the pseudohalide ions ($N_3^-$, $NCS^-$, $NCO^-$, $N(NC)_2^-$) are versatile ligands that can bind transition metal ions in a variety of ways. These anions can act as monodentate ligands and as bridging ligands leading to the formation of mononuclear and polynuclear species with different dimensionalities and nuclearities. Among these, the azide- and thiocyanate-containing metal complexes are considered to be the most investigated systems because of their diverse structures and applications in magnetic materials. Having two different donor atoms $SCN^-$ can coordinate to metals through either the nitrogen or the sulphur atom, or both.

J. G. Małecki (✉) · B. Machura · A. Świtlicka
Department of Crystallography, Institute of Chemistry, University of Silesia, 9th Szkolna St., 40-006 Katowice, Poland
e-mail: gmalecki@us.edu.pl

In agreement with the hard soft acid base (HSAB) $SCN^-$ ion coordinate to hard acids ($Mn^{2+}$, $Co^{2+}$ and $Ni^{2+}$) through nitrogen atom, and the uncoordinated sulphur atom is involved in hydrogen bonds and sometimes involved in S···S interactions. If the transition metal centre is soft acid ($Cd^{2+}$, $Cu^{+}$ and $Hg^{2+}$) $SCN^-$ ligand binds to central ion through sulphur atom. Different bridging modes of the thiocyanato ligand can generate various types of supramolecular structures with particular properties. Thiocyanato bridges play an important role in the magnetic exchange pathways between paramagnetic centres. $SCN^-$ ion possesses polarizable $\pi$ system, the electron is dislocated and it may act as a mediator for the magnetic interaction between the paramagnetic transition metal centres. The geometry and coordination mode of $NCS^-$ in *3d* metal complexes is strongly influenced by the electronic and steric effects around central ion [5–11]. Thiocyanate complexes with the formula of $[M(NCS)_2L_4]$, where L is a N-heteroaromatic ligand such as pyridine, are called Werner-type complexes and are well known. The complexes are interesting because of their architectures organised by non-covalent contacts as hydrogen bonds, $\pi$–$\pi$ stacking interaction and simplicity of preparation and their catalytic efficiency [12, 13]. Their interesting structural properties and potential application are attractive in studies of magnetism or magnetic exchange ions.

In this article, we present the synthesis, crystal, molecular, electronic structures and the spectroscopy characterisation of the manganese(II), nickel(II) and copper(II) complexes with 5,6-diphenyl-3-(2-pyridyl)-1,2,4-triazine ligands. The electronic structure of the studied complexes has been determined with the density functional theory (DFT) method, and employed for discussion of the bonding properties. Currently, density functional theory (DFT) is commonly used to examine the electronic structure of transition metal complexes. It meets with the requirements of being accurate, easy to use and fast enough to allow the study of relatively large molecules of transition metal complexes.

## Experimental

All reagents used for the synthesis of the complex are commercially available and were used without further purification.

Synthesis of $[M(SCN)_2(pytz)_2]$, where M = Mn(II) (1), Cu(II) (3) and $[NiCl_2(pytz)_2]\cdot 2CH_3OH$ (2) complexes

These complexes were synthesized in the reaction between $MnCl_2\cdot 4H_2O$, $NiCl_2\cdot 6H_2O$, $CuCl_2\cdot 2H_2O$, $NH_4SCN$ (except the nickel(II) complex) and stoichiometric volumes of 5,6-diphenyl-3-(2-pyridyl)-1,2,4-triazine (pytz) in methanolic solution (50 $cm^{-3}$). The mixtures of the compounds were refluxed for 0.5 h. After this time, the volume of the solvent was reduced to about 20 $cm^3$; the solution was cooled and left out to slow evaporation.

*$[Mn(SCN)_2(pytz)_2]$ (**1**)*

Yield 84%. IR (KBr): 3064 $\nu_{ArH}$; 2068 $\nu_{(CN\ from\ SCN)}$; 1599 $\nu_{CN}$, 1572 $\nu_{C=C}$; 1481, 1374 $\delta_{(C–CH\ in\ the\ plane)}$; 1446 $\nu_{ArH}$; 1121 $\delta_{(C–CH\ in\ the\ plane)}$; 1009 $\delta_{(C–H\ out\ of\ the\ plane)}$; 798 $\delta_{(C–C\ out\ of\ the\ plane)}$; 770 $\nu_{(SC\ from\ SCN)}$, 698 $\delta_{(C–C\ in\ the\ plane)}$; 538 $\delta_{(NCS)}$, 414 $\nu_{(Mn–Npy)}$. UV–vis (methanol; log$\varepsilon$): 498.4 (0.98), 439.0 (1.01), 360.5(1.24), 283.0 (3.76), 234.0 (2.11), 206.5 (4.27).

*$[NiCl_2(pytz)_2]\cdot 2CH_3OH$ (**2**)*

Yield 91%. IR (KBr): 3359 $\nu_{OH}$; 3060 $\nu_{ArH}$; 1601 $\nu_{CN}$, 1580 $\nu_{C=C}$; 1517, 1255 $\delta_{(C–CH\ in\ the\ plane)}$; 1446 $\nu_{Ph}$; 1013 $\delta_{(C–CH\ in\ the\ plane)}$; 924 $\delta_{(C–H\ out\ of\ the\ plane)}$; 770 $\delta_{(C–C\ in\ the\ plane)}$. UV–vis (methanol; log$\varepsilon$): 887.0 (0.78), 790.2 (0.81), 494.0 (1.32), 331.3 (2.79), 300.0 (3.89), 235.0 (2.13), 205.4 (4.28).

*$[Cu(SCN)_2(pytz)_2]$ (**3**)*

Yield 62%. IR (KBr): 3097 $\nu_{ArH}$; 2080 $\nu_{(CN\ from\ SCN)}$; 1612 $\nu_{CN}$, 1591 $\nu_{C=C}$; 1483, 1368 $\delta_{(C–CH\ in\ the\ plane)}$; 1445 $\nu_{Ph}$; 1039 $\delta_{(C–CH\ in\ the\ plane)}$; 1007 $\delta_{(C–H\ out\ of\ the\ plane)}$; 811 $\delta_{(C–C\ out\ of\ the\ plane)}$, 760 $\nu_{(SC\ from\ SCN)}$; 693 $\delta_{(C–C\ in\ the\ plane)}$; 536 $\delta_{(NCS)}$. UV–vis (methanol; log$\varepsilon$): 752.5 (1.03), 433.5 (1.16), 360.5 (1.21), 300.0 (1.71), 232.5 (2.17), 207.0 (4.32).

### *Physical measurements*

Infrared spectra were recorded on a Nicolet Magna 560 spectrophotometer in the spectral range of 4000 ÷ 400 $cm^{-1}$ with the sample in the form of KBr pellet. Electronic spectra were measured on a Lab Alliance UV–VIS 8500 spectrophotometer in the range of 1100 ÷ 180 nm in methanol solution. EPR spectra were recorded in powder sample at 295 K on a Bruker EMX-10 spectrometer using 100 kHz field modulation.

### *DFT calculations*

The calculations were carried out using Gaussian09 [14] program. The DFT/B3LYP [15, 16] method was used for the geometry optimisation and electronic structure determination. The calculations were performed using the polarisation functions for all atoms: 6–311 g**—manganese, nickel,

copper, 6–31 g**—carbon, nitrogen, sulphur and 6–31 g—hydrogen. Natural bond orbital (NBO) calculations were performed with the NBO code [17] included in Gaussian09. The contribution of a group to a molecular orbital was calculated using Mulliken population analysis. GaussSum 2.2 [18] was used to calculate group contributions to the molecular orbitals and to prepare the density of states (DOS) and overlap population density of states (OPDOS) spectra. The OPDOS spectra were created by convoluting the molecular orbital information with Gaussian curves of unit height and full width at half maximum (FWHM) of 0.3 eV. Mayer bond orders were calculated with use of QMForge program [19].

*Crystal structures determination and refinement*

The crystals of $[Mn(SCN)_2(pytriaz)_2]$ (**1**), $[NiCl_2(pytriaz)_2]\cdot 2CH_3OH$ (**2**) and $[Cu(SCN)_2(pytriaz)_2]$ (**3**) were mounted in turn on a Xcalibur, Atlas, Gemini ultra Oxford Diffraction automatic diffractometer equipped with a CCD detector, and used for data collection. X-ray intensity data were collected with graphite monochromated Mo K$\alpha$ radiation ($\lambda = 0.71073$ Å) at temperature of 298.0(2) K (**1**, **2**) or 150.0(2) K (**3**), with $\omega$ scan mode. Ewald sphere reflections were collected up to $2\theta = 50.10$. The unit cell parameters were determined from least-squares refinement of the setting angles of 8420, 9214 and 5146 strongest reflections for complexes (**1**), (**2**) and (**3**), respectively. Details concerning crystal data and refinement are shown in Table 1. During the data reduction, the decay correction coefficient was taken into account. Lorentz, polarisation and numerical absorption corrections were applied. The structures were solved by direct method. All the non-hydrogen atoms were refined anisotropically using full-matrix, least-squares technique on $F^2$. All the hydrogen atoms were found from difference Fourier synthesis after four cycles of anisotropic refinement, and refined as "riding" on the adjacent atom with individual isotropic temperature factor equal to 1.2 times the value of equivalent temperature factor of the parent atom, with geometry idealisation after each cycle. Olex2 [20] program was used for all the calculations. Atomic scattering factors were those incorporated in the computer programs.

## Results and discussion

The reactions of the chloride salts of manganese(II), nickel(II) and copper(II) with 5,6-diphenyl-3-(2-pyridyl)-1,2,4-triazine (pytz) and ammonium thiocyanate in the case of complexes **1** and **3** have been carried out. Refluxing the starting metal(II) salt with the ligands in methanol leads to hexacoordinate complexes with good yields. Infrared spectra of the complexes present characteristic bands due to ligands vibrations.

The stretching modes of the aryl C–H bond display maxima at 3064, 3060 and 3097 $cm^{-1}$ for complexes (**1**), (**2**), and (**3**) respectively. In the spectrum of complex (**2**) band with maximum at 3359 $cm^{-1}$ is assigned to hydroxyl group of the methanol molecules. The $\nu_{C=N}$ band of pyridine ring appears at about 1600 $cm^{-1}$. The $\nu_{CN}$, $\nu_{CS}$ and $\delta_{NCS}$ frequencies of isothiocyanato ligands present maxima at 2068 $cm^{-1}$ (**1**), 2080 $cm^{-1}$ (**3**), 770, 760 $cm^{-1}$ and 538, 536 $cm^{-1}$, respectively, and it is in good agreement with the end-on NCS coordination. The coordination modes of thiocyanate ligands in the studied complexes are indeterminable from the IR spectral data of these compounds. For N-bonded complexes, generally the C–N stretching band is in a lower region around 2050 $cm^{-1}$ than that of 2100 $cm^{-1}$ for S-bonded complexes. However, the frequencies of the bands are sensitive to other factors like coexisting ligands and the structure of the compounds were determined using X-ray analysis. While the M–S–C angles of S-bonded thiocyanato ligand in complexes are bent around 110°, the M–N–C angles of N-bonded isothiocyanato ligands are close to linear.

The complexes (**1**) and (**3**) crystallize in the monoclinic space group *C*2/*c*. The complex (**2**) crystallizes in triclinic *P*-1 space group. Details concerning crystal data and refinement are shown in Table 1. The molecular structures of the studied compounds are shown in Fig. 1. The selected bond lengths and angles are listed in Table 2.

In all the complexes, central ions have octahedral environment and lie on the inversion centre in the structures of the complexes. The coordination octahedra have angular deviations (maximum 12.5°) connected with N–M–N angles. The C–N and C–S bond length values fall in the 1.153(2)–1.158(2) Å and 1.620(2)–1.632(19) Å ranges for the complexes (**1**) and (**3**), similar to those observed for isothiocyanate complexes. The $M–N_{(pytz)}$ and Ni–Cl distances are normal and comparable with distances in other complexes containing the N–heterocyclic ligands. The Mn–N–C angles about 162° are in a good agreement with those found for $M(3d)^{2+}$ complexes having bent terminally bonded NCS ligand (141°–174°). The isothiocyanate ligands are almost linear (178°). The conformations of molecules (**2**) and (**3**) are stabilized by intra- and intermolecular hydrogen bond, and the hydrogen bonds are shown in Table 3. Additionally, the $\pi$-stacking interactions in the crystal structures of the complexes are observed. In Fig. 2, the networks formed by the hydrogen bonds and $\pi$-stacking interactions in the complexes are shown.

To form an insight in the electronic structures and bonding properties of the complexes, the DFT calculations were carried out. Before the calculations of electronic structures of the complexes, their geometries were

**Table 1** Crystal data and structure refinement details of $[Mn(SCN)_2(pytriaz)_2]$ (**1**), $[NiCl_2(pytriaz)_2]\cdot 2CH_3OH$ (**2**) and $[Cu(SCN)_2(pytriaz)_2]$ (**3**) complexes

| | **1** | **2** | **3** |
|---|---|---|---|
| Empirical formula | $C_42H_28MnN_{10}S_2$ | $C_42H_36Cl_2N_8NiO_2$ | $C_42H_28CuN_{10}S_2$ |
| Formula weight | 791.80 | 814.38 | 800.40 |
| Temperature (K) | 298.0(2) | 298.0(2) | 150.0(2) |
| Crystal system | Monoclinic | Triclinic | Monoclinic |
| Space group | *C*2/*c* | *P*-1 | *C*2/*c* |
| Unit cell dimensions | | | |
| a [Å] | 15.7209(5) | 8.6196(4) | 15.3773(10) |
| b [Å] | 9.3014(3) | 9.0767(4) | 9.2685(6) |
| c [Å] | 26.3303(8) | 13.4248(5) | 26.3299(18) |
| $\alpha$ | 90 | 82.692(3) | 90 |
| $\beta$ | 96.214(3) | 78.916(4) | 97.127(6) |
| $\gamma$ | 90 | 70.364(4) | 90 |
| Volume ($Å^3$) | 3827.6(2) | 968.56(7) | 3723.7(4) |
| *Z* | 4 | 1 | 4 |
| Calculated density ($Mg/m^3$) | 1.374 | 1.396 | 1.428 |
| Absorption coefficient ($mm^{-1}$) | 0.500 | 0.687 | 0.746 |
| F(000) | 1628 | 422 | 1644 |
| Crystal dimensions (mm) | 0 × 0 × 0 | 0.26 × 0.11 × 0.05 | 0 × 0 × 0 |
| $\theta$ range for data collection (°) | 3.55–25.00 | 3.53–25.04 | 2.57–25.05 |
| Index ranges | $-18 \le h \le 18$ | $-10 \le h \le 10$ | $-14 \le h \le 18$ |
| | $-11 \le k \le 11$ | $-10 \le k \le 10$ | $-9 \le k \le 11$ |
| | $-31 \le l \le 31$ | $-15 \le l \le 15$ | $-30 \le l \le 30$ |
| Reflections collected | 18481 | 17115 | 11958 |
| Independent reflections | 3347 [$R_{(int)} = 0.0372$] | 3385 [$R_{(int)} = 0.0638$] | 3288 [$R_{(int)} = 0.0251$] |
| Data/restraints/parameters | 3347/0/250 | 3385/0/252 | 3288/0/250 |
| Goodness-of-fit on $F^2$ | 1.043 | 0.996 | 0.955 |
| Final *R* indices [$I > 2\sigma(I)$] | $R_1 = 0.0295$ | $R_1 = 0.0531$ | $R_1 = 0.0261$ |
| | $wR_2 = 0.0742$ | $wR_2 = 0.1360$ | $wR_2 = 0.0674$ |
| R indices (all data) | $R_1 = 0.0429$ | $R_1 = 0.0729$ | $R_1 = 0.0342$ |
| | $wR_2 = 0.0766$ | $wR_2 = 0.1435$ | $wR_2 = 0.0689$ |
| Largest diff. peak and hole | 0.249 and −0.240 | 0.737 and −0.472 | 0.312 and −0.213 |

optimised in triplet states using the DFT method with the B3LYP functional. From the data shown in Table 2, one may see that the elongation of bonds in gas phase optimised geometry do not outrun 0.1 Å and the largest differences in angles were found for Mn(1)–C(1)–N(1) 3.12°. Based on the optimised geometry of complex (**3**) the IR spectrum was calculated and compared with the experimental one. As one can see from Fig. 3, the experimental and calculated IR spectra are close each other besides the hydrogen bonds range ($\sim$3500 $cm^{-1}$) which are poorly interpreted by the single point calculations in Gaussian.

The formal charges of central ions are +2 in the complexes and the calculated charges on the central atoms, obtained from natural population analysis, are approximately 1.61 on $Mn^{2+}$, 1.40 on $Ni^{2+}$ and 1.45 on $Cu^{2+}$. The charges on the N-donor atoms from isothiocyanate ligands are −0.8 in complexes (**1**) and (**3**), chloride ions in complex (**2**) have charges close to −0.8 and those on the pytz are −0.5 and −0.3 on pyridine and triazole nitrogen donor atoms, respectively. These are the results of charges donation from the ligands to the metal centre. The conclusion confirms the second-order perturbation analysis from NBO. The stabilization energy calculated in this analysis shows that the lone pairs localised on the N-donor atoms of thiocyanate ligands donate the charge to the $Mn^{2+}$ and $Cu^{2+}$ ions *d* orbitals, and the stabilization energy ($\Delta E_{ij}$) is 69.56 and 92.14 kcal/mol, respectively. The back donation charges form metal to $NCS^-$ ligands stabilise the molecules (**1**) and (**3**) by 37.92 and 46.65 kcal/mol. The energies in the complex (**2**) connected with charge flow between chloride ions and central nickel(II) atom averaging to 12.04 (Ni → Cl) and 99.78 (Cl → Ni). The

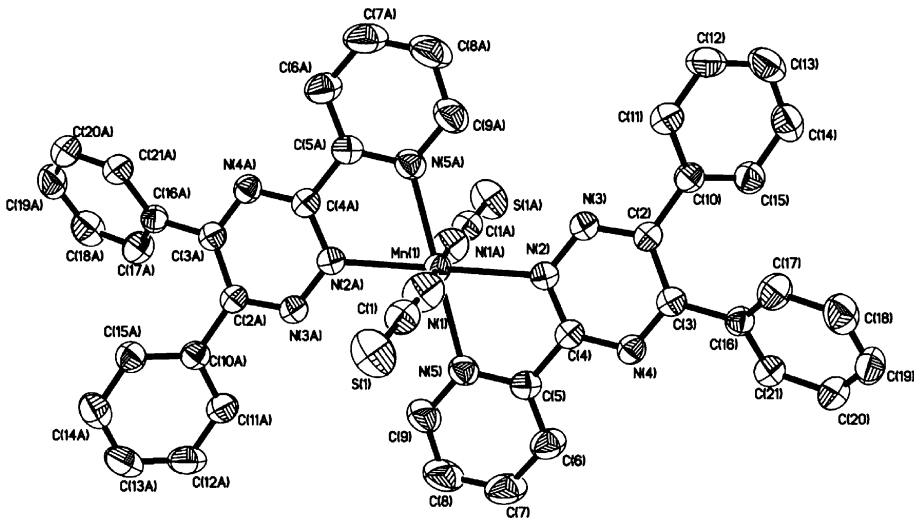


**1**

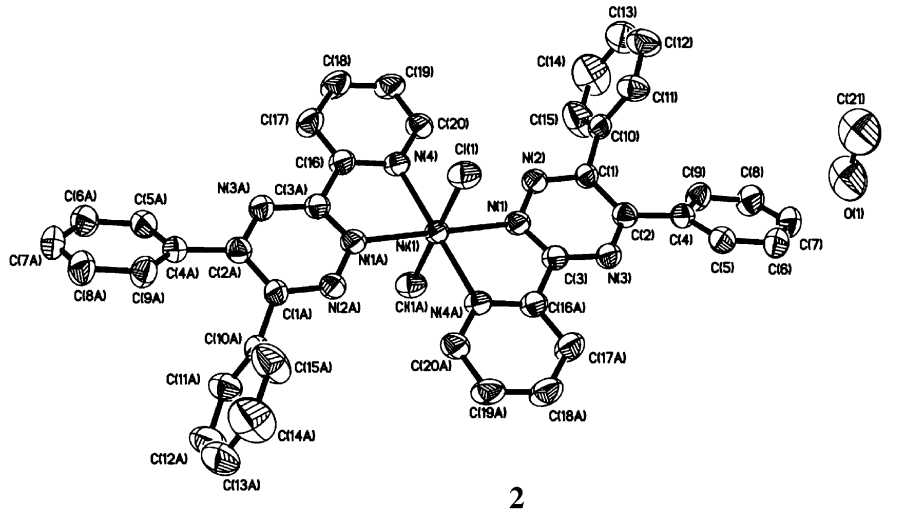


**2**

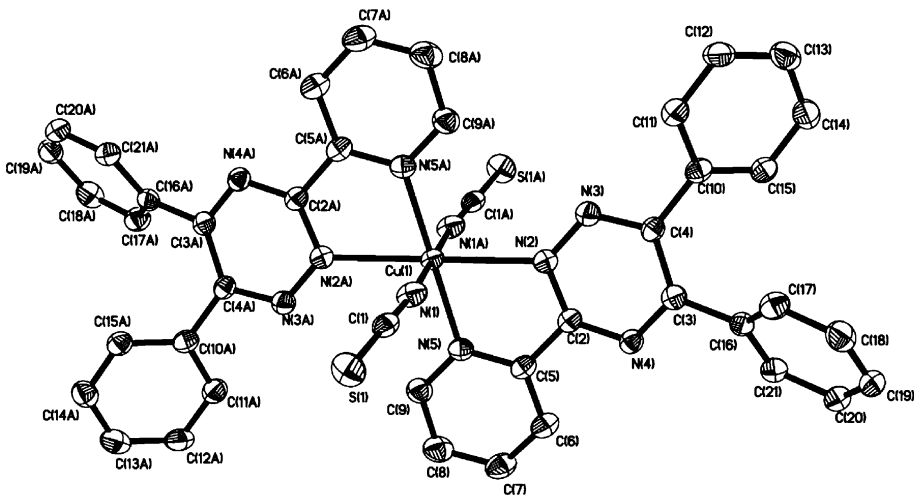


**3**

**Fig. 1** ORTEP drawing of $[Mn(SCN)_2(pytriaz)_2]$ (**1**), $[NiCl_2(pytriaz)_2]\cdot CH_3OH$ (**2**), $[Cu(SCN)_2(pytriaz)_2]$ (**3**) with 50% probability displacement ellipsoids. Hydrogen atoms are omitted for clarity

**Table 2** Selected bond lengths (Å) and angles (°) for $[Mn(SCN)_2(pytriaz)_2]$ (**1**), $[NiCl_2(pytriaz)_2]$ (**2**) and $[Cu(SCN)_2(pytriaz)_2]$ (**3**) complexes

| | **1** | | **2** | | **3** | |
|---|---|---|---|---|---|---|
| | Exp | Calc | Exp | Calc | Exp | Calc |
| Bond lengths (Å) | | | | | | |
| M(1)–N(1) | 2.1539(17) | 2.098 | 2.088(2) | 2.117 | 1.975(16) | 1.948 |
| M(1)–N(2) | 2.2542(13) | 2.336 | | | 2.333(14) | 2.436 |
| M(1)–N(4) | | | 2.125(2) | 2.127 | | |
| M(1)–N(5) | 2.2609(14) | 2.339 | | | 2.042(14) | 2.082 |
| M(1)–Cl(1) | | | 2.402(8) | 2.396 | | |
| N(1)–C(1) | 1.153(2) | 1.187 | | | 1.158(2) | 1.185 |
| S(1)–C(1) | 1.620(2) | 1.629 | | | 1.632(19) | 1.629 |
| Angles (°) | | | | | | |
| N(1)–M(1)–N(2) | 89.78(6) | 90.89 | | | 90.58(6) | 90.33 |
| N(1)–M(1)–N(4) | | | 102.56(9) | 102.33 | | |
| N(1)–M(1)–N(5) | 88.83(6) | 89.10 | | | 89.53(6) | 89.70 |
| N(2)–M(1)–N(5) | 73.09(5) | 70.97 | | | 75.74(5) | 73.80 |
| N(1)–M(1)–Cl(1) | | | 86.57(7) | 88.74 | | |
| N(4)–M(1)–Cl(1) | | | 91.40(7) | 91.26 | | |
| M(1)–N(1)–C(1) | 161.72(17) | 164.84 | | | 162.30(15) | 164.20 |
| N(1)–C(1)–S(1) | 177.90(19) | 179.97 | | | 178.05(18) | 179.98 |

*M* Mn in **1**, *Ni* in **2** and *Cu* in **3**

**Table 3** Hydrogen bonds for $[NiCl_2(pytz)_2]\cdot 2CH_3OH$ (**2**) and $[Cu(SCN)_2(pytriaz)_2]$ (**3**) complexes (Å and °)

| D–H···A | d(D–H) | d(H···A) | d(D···A) | < (DHA) |
|---|---|---|---|---|
| **2** | | | | |
| C(20)–H(20)···N(2) | 0.93 | 2.40 | 3.179(4) | 140.7 |
| O(1)–H(1)···Cl(2) #1 | 0.82 | 2.33 | 3.129(3) | 164.9 |
| **3** | | | | |
| C(9)–H(17)···N(3) #2 | 0.93 | 2.54 | 3.393(2) | 153.3 |

Symmetry transformations used to generate equivalent atoms: #1 $x$, $1 + y$, $-1 + z$; #2 $1/2 - x$, $3/2 - y$, $-z$

stabilisation energies associated with the charge donation from central ions to the N-donor ligands (pytz) are equal to 35.92 kcal/mol for (**1**), 29.82 for (**2**) and 66.76 kcal/mol for complex (**3**). The stabilization energy of the charge donation from the pytz to the antibonding *d* orbitals is 49.61 kcal/mol for complex (**1**), 91.10 for (**2**) and 77.35 kcal/mol for (**3**). The NBO analyses suggest the ionic character of bonds between central ions and ligands in the complexes. The calculated Mayer bond orders for M–NCS/Cl are equal to 0.30 and the values for bonds between pytz ligands and manganese(II) are 0.14, 0.23 for Ni–N(pytz) and in complex (**3**) the order of bond between pyridine nitrogen donor and copper(II) is more covalent (0.28) that that between triazole moiety and Cu(II) (0.10). The bond orders pointed out the ionic character bonds in the complexes.

The atomic charge calculations may describe the relocation of electron density of the compounds. The electron distribution is not apparent from the partial atomic charges, so the plot of the electrostatic potential for the complex **3** is shown in Fig. 4. The isoelectronic contours are plotted at 0.05 a.u. (31 kcal/mol). The colour code of these maps is in the range of 0.05 a.u. (deepest red) to −0.005 a.u. (deepest blue), where blue indicates the strongest attraction and red indicates the strongest repulsion. Regions of negative $V(r)$ are usually associated with the lone pair of electronegative atoms. The negative potential in the compounds wrap thiocyanate ligands and nitrogen atoms in the 5,6-diphenyl-3-(2-pyridyl)-1,2,4-triazine ligands. As one can see from Fig. 4, negative potentials on sulphur atoms in the complex are smaller than the ones on nitrogen atoms. The natural charges obtained from NBO analysis are $N_{(NCS)}$ −0.7, $S_{(NCS)}$ −0.3 and $N_{(py)}$ −0.5, $N_{(tz)}$ −0.3. That is why, and additionally because of steric hindrance exerted by phenyl rings in the ligands, the studied complexes do not form polymeric systems with $NCS^-$ connector.

In all the complexes, the HOMO orbitals are localised on thiocyanate or chloride ligands with contribution of *d* metal orbitals (13%). The *d* orbitals of central ions play a significant role (32–55%) in the lower HOMO–4/5 MOs in the complexes. The LUMO orbitals are localised on the pytz ligands in all complexes. In virtual molecular orbitals the *d* cental ions orbitals are visible in the ($\beta$ spin) Lumo + 14/15 (28–90%) in complex (**1**), LUMO + 10/12 (36%, 77%) in (**2**) and Lumo + 4 (70%) in (**3**). Because in

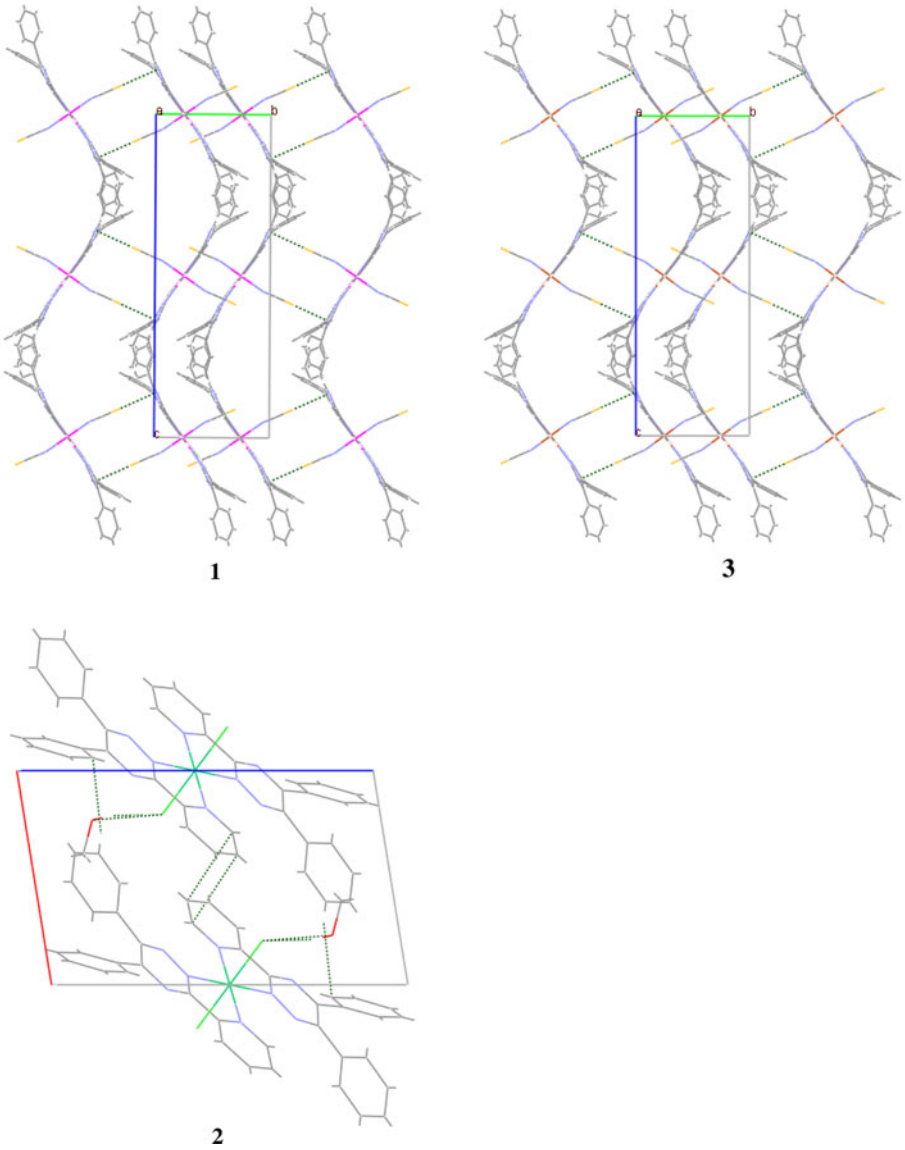


**Fig. 2** The crystal packing of complexes **1**–**3** viewing down the *a* axis with hydrogen bonds indicated by *dotted lines*

the frontier region, neighbouring orbitals may be a quasi-degeneracy of the energetic levels, consideration of only the HOMO and LUMO may not yield a realistic description of the frontier orbitals. For this reason, the density of states (DOS) in terms of Mulliken population analysis was calculated using the GaussSum program. The results provide a pictorial representation of MOs compositions. The DOS diagrams for complexes (**2**) and (**3**) are shown in Fig. 5, and they may enable us to ascertain the orbital composition characteristics with respect to the particular fragments. As one may see from the DOS diagrams, pytz ligands play significant role in the virtual frontier and in the lower occupied molecular orbitals. The chloride contributes in wider range HOMO orbitals than pseudohalide $NCS^-$ ligands. Additionally, the complexes with isothiocyanate ligands have smaller HOMO–LUMO gap when compared with chloride ligands (**1**: 2.08 eV; **2**: 2.40 eV; **3**: 2.22 eV). The HOMO term is shifted to higher energy by pseudohalide ligands which have an impact on the contribution of *d* orbitals of central ions in the HOMO orbitals. The values are small for $SNC^-$ complexes indicating that the M–NCS bonds are more covalent than M–Cl bond. This is because of the difference in bonding of $Cl^-$ and $NCS^-$. On the M–NSC complexes, the $d_z^2$ orbital (assuming *z*-axis coincides with M–Cl or M–NCS are filled) can donate electron density to the metal whereas the back donation to chloride ligands is difficult.

Electronic spectrum of the Mn(II) complex (**1**) exhibits weak intensity absorption bands with maxima at $\nu_1$: 20064, $\nu_2$: 22779, $\nu_3$: 27739, $\nu_4$: 35335 $cm^{-1}$. These bands may be assigned to transitions: $\nu_1$: $^6A_{1g} \rightarrow {}^4T_{1g}(^4G)$, $\nu_2$: $^6A_{1g} \rightarrow {}^4E_g/{}^4A_{1g}(^4G)(10B + 5C)$, $\nu_3$: $^6A_{1g} \rightarrow {}^4E_g(^4D)(17B + 5C)$ and $\nu_4$: $^6A_{1g} \rightarrow {}^4T_{1g}(^4P)(7B + 7C)$. The parameters *B* and *C* were calculated from the second and third

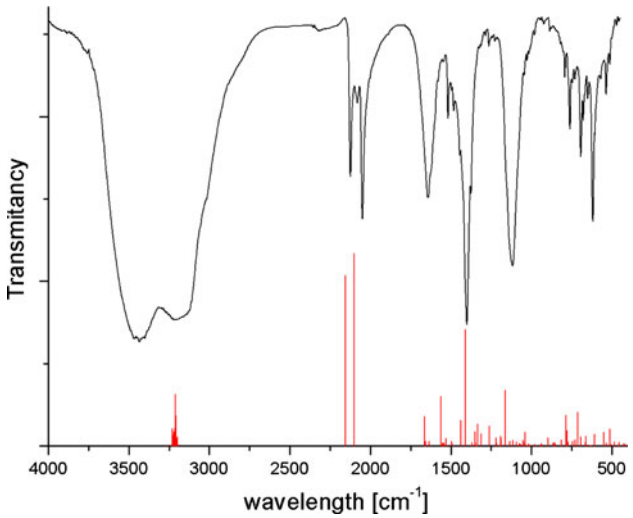


**Fig. 3** Experimental IR spectrum and calculated IR transitions of $[Cu(SCN)_2(pytriaz)_2]$ (**3**) complex

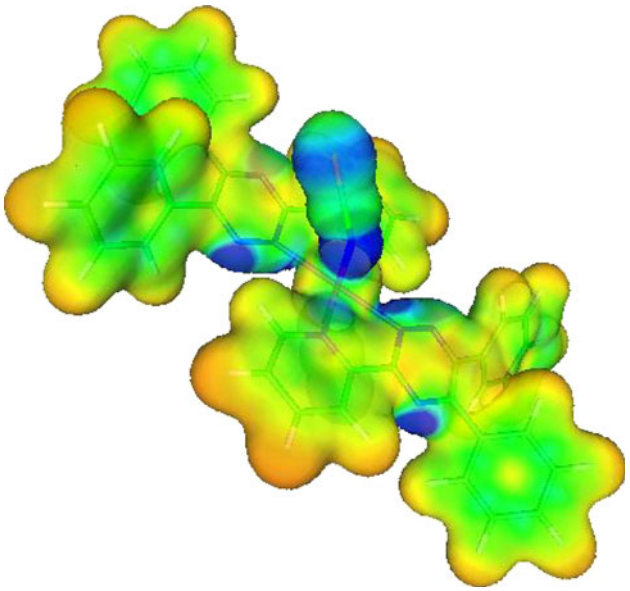

**Fig. 4** Electrostatic potential (ESP) surface of complex **3**. ESP surface is shown both in space (with positive and negative regions shown in *red* and *blue*, respectively) and mapped on electron densities (isovalue = 0.05) of the molecule (ESP colour scale is such that $\delta^+ \rightarrow \delta^-$ in the direction *red* → *blue*) (Color figure online)

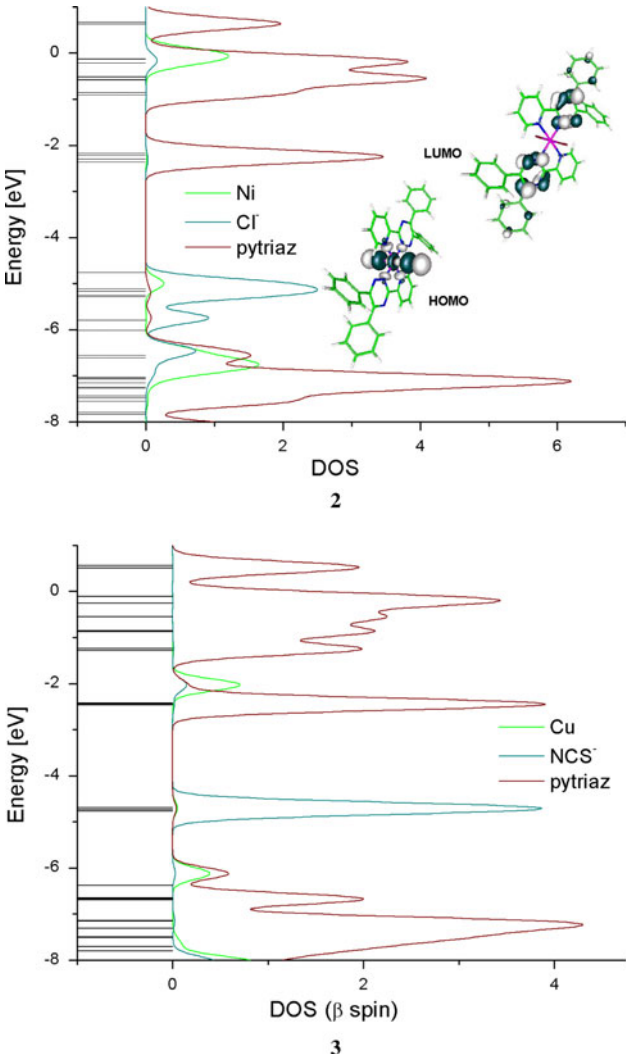


**Fig. 5** The density of states (DOS) diagrams for $[NiCl_2(pytriaz)_2]$ (**2**) and $[Cu(SCN)_2(pytriaz)_2]$ (**3**) complexes

transitions because these transitions are free from the crystal field splitting and depend only on $B$ and $C$ parameters. The values of Racah parameters are equal to $B = 709$ cm$^{-1}$ and $C = 3138$ cm$^{-1}$. Based on the maximum of first transition the crystal field splitting parameters 10 Dq has been calculated and amount to 10558 cm$^{-1}$.

The lowest state of the nickel(II) ion is $^3$F term, which splits into $^3A_{2g}$, $^3T_{2g}$ and $^3T_{1g}$ terms in the field with $O_h$ symmetry. The studied complexes have $D_{4h}$ point group symmetry, and in this symmetry $^3T_{2g}$ and $^3T_{1g}$ terms split into singlet $^3A_{2g}$ and $^3B_{2g}$ and doublet $^3E_g$ levels each. As a consequence, the first and second spin allowed transition bands observed on the UV–vis spectra of the complexes are assigned to $^3T_{2g}(^3F) \rightarrow {}^3A_{2g}(^3F)$ and $^3T_{1g}(^3F) \rightarrow {}^3A_{2g}(^3F)$, respectively. The third absorption band results from a spin allowed transition $^3T_{1g}(^3P) \rightarrow {}^3A_{2g}(^3F)$. The value of the ligand field parameter 10 Dq, calculated on the basis of electronic bands positions for the complex (given in "Experimental"), is equal to 10Dq = 11234 cm$^{-1}$. Racah parameters $B$ and $C$ are equal to 674 and 3174 cm$^{-1}$, respectively. The Racah parameter $B$ for a metal ion varies as a function of the ligand bound to the ion. The value of this parameter will be always lower for the complexed ion than that for the free ion. The reduction of the value of $B$ is related to the extent of metal–ligand bond covalency. The metal–ligand bond becomes partially covalent when the $d$-orbitals overlap with the ligand orbitals. As a result,

the interelectronic repulsion within the *d*-orbitals decreases and *B* value is lowered. The ratio $B/B_0 = \beta$ gives a measure of covalency in the metal–ligand bond. Taking into account that the $B_0$ for Mn(II) free ion is 786 $cm^{-1}$ and for Ni(II) is 1041 $cm^{-1}$ the nepheloauxetic parameters calculated for the complexes are $\beta = 0.90$ and 0.65 for complexes (**1**) and (**2**), respectively. The values confirm ionic character of manganese/nickel–ligands $\sigma$ bonds in the complexes and are in accordance with the calculated Mayer bond orders.

On the UV spectrum of complex (**2**) was recorded the band with maximum at 790.2 nm. It is ascribed to $^1E_g(^1D)$ term in $O_h$ symmetry, which separates in the $D_{4h}$ symmetry into $^1A_{1g}$ and $^1B_{1g}$ levels. This indicates that the band correspond to spin forbidden $^1A_{1g}/^1B_{1g}(^1D) \rightarrow {}^3A_{2g}(^3F)$ transitions. For the calculated Dq/*B* ratio (1.67) in the Tanabe–Sugano diagram for $d^8$ ions in octahedral coordination one can see, in Fig. 6, that the $^1E_g(^1D)$ singlet state is lower than the triplet $^3T_{1g}(^3F)$ term which confirms the band position in the spectra. Additionally close to the Dq/*B* ratio of the complex the singlet and triplet terms intersect which explain the higher intensity of the spin forbidden band than that $^3T_{2g}(^3F) \rightarrow {}^3A_{2g}(^3F)$ transition.

The electronic spectrum of copper(II) complex (**3**) shows three bands with maxima at 13289, 23068 and 27738 $cm^{-1}$ which may be considered to the following spin allowed transitions: $^2B_{1g} \rightarrow {}^2A_{1g}(d_{x^2-y^2} \rightarrow d_{z^2})$, $^2B_{1g} \rightarrow {}^2B_{2g}(d_{x^2-y^2} \rightarrow d_{zy})$ and $^2B \rightarrow {}^2E_g(d_{x^2-y^2} \rightarrow d_{zy}, d_{yz})$ and suggest $D_{4h}$ symmetry. For this complex the nature of the transitions observed in the UV–Vis spectrum has been studied by the time-dependent density functional (TDDFT) method based on the optimised geometry, in gas phase without any symmetry restrictions, in the doublet state. The experimental spectrum with the calculated transitions is depicted in Fig. 6. The TDDFT/PCM calculations show that the two longest wavelength experimental bands of (**3**) at 752.5 (13 289 $cm^{-1}$) and 433.5 nm (23 068 $cm^{-1}$) originate from the transitions between $\beta$-spin HOMO, HOMO-1, HOMO-23 orbitals and $\beta$-spin LUMO orbital. As can be seen from Fig. 5, in the LUMO orbital with $\beta$ spin the Cu $d_{x^2-y^2}$ orbital participates in character and the $\beta$-spin HOMO and HOMO-1 orbitals are composed of the $\pi$-bonding orbitals of isothiocyanate with some contributions of 5,6-diphenyl-3-(2-pyridyl)-1,2,4-triazine orbitals. The HOMO-23 is ligand (SCN and pytz) $\pi$-bonding orbitals with some contribution of $d_{Cu}$ orbitals. Accordingly, the transitions assigned to the longest wavelength experimental band can be seen as mixed SCN/pytz → Cu (*LMCT*) and $d \rightarrow d$ (*LF*). Thus, no "clear" *d–d* transition bands occur in the low-lying energy region for the complex. The reason for this is probably because of the pytz ligand provides high-lying occupied $\pi$-bonding orbitals, and as a result the high-lying occupied orbitals are composed of the $\pi$-bonding orbitals of 5,6-diphenyl-3-(2-

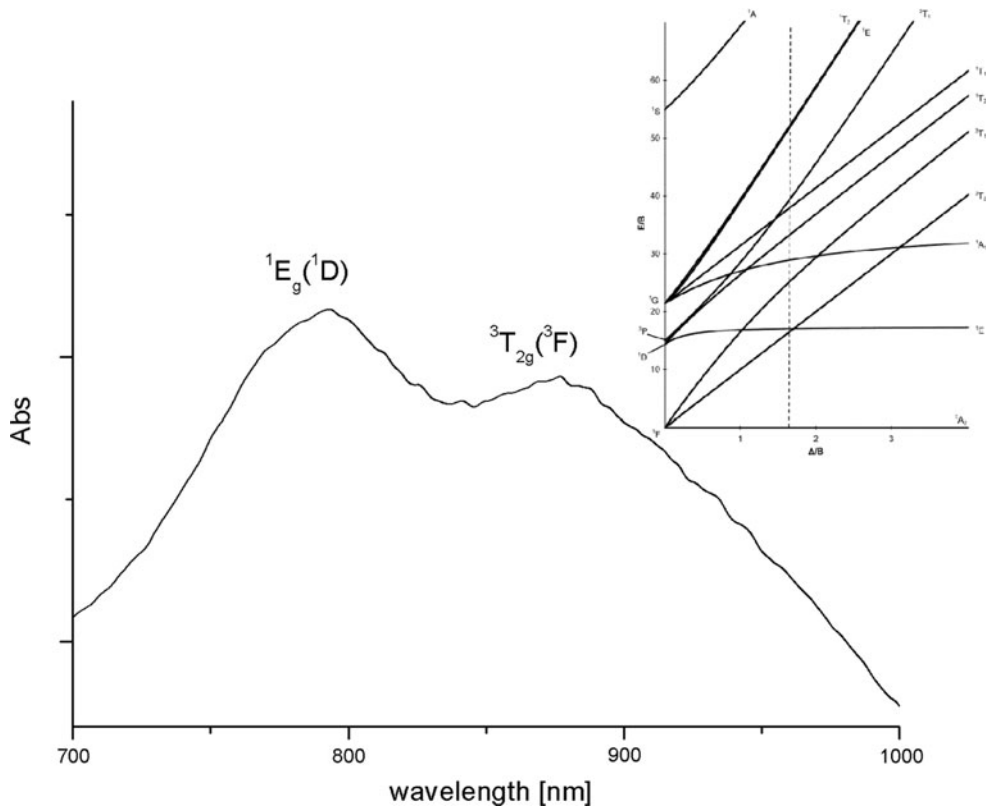


**Fig. 6** The part of UV–vis spectrum of $[NiCl_2(pytriaz)_2]$ (**2**) complex with Tanabe–Sugano diagram for $d^8$ ions in octahedral coordination

pyridyl)-1,2,4-triazine. The experimental bands with maxima at 232.5 and 207.0 nm are attributed to the *intraligand* (IL) ($\pi_{(pytz)} \rightarrow \pi^*_{(pytz)}$) and *ligand–ligand charge transfer* ($\pi_{(SCN)} \rightarrow \pi^*_{(pytz)}$) transitions (Fig. 7).

An emission property of the complex (**2**) has been examined in the methanol solution (with concentration of $5 \times 10^{-4}$ mol/dm$^3$) at room temperature. The excitation was executed at 494 nm, i.e., for the maximum of absorption band which may be assigned to the combination of $d \rightarrow d$, MLCT ($d\pi_{(Ni)} \rightarrow \pi^*_{(pytz)}$) and $^1$ClLCT ($n$(Cl) $\rightarrow \pi^*$) transitions. The low intense emission with maximum at 581 nm was observed (Fig. 8).

The X-band EPR spectra of the complexes were recorded at room temperature at frequency 9.8 GHz, in polycrystalline form (Fig. 9). On the spectrum of manganese(II) complex (**1**) is visible two broad signals with g values of 3.40 and 1.96. The EPR spectrum of polycrystalline sample of complex **3** exhibit signals with $g_{\|} = 2.20$ and $g_{\perp} = 2.08$. The ordering of $g$ values $g_{\|} > g_{\perp} > 2.0023$ observed for the copper(II) complex indicates that the unpaired electron most likely resides in their $d_x{}^2{}_{-y}{}^2$ orbital which is consistent with $^2B_{1g}$ ground state. The fact that the $g_{\|}$ is little smaller than 2.3 is an indication of some ionic character of bonding in the complex as in the case of complexes (**1**) and (**2**) [21–23]. According to Hathaway and Billing [24], if the geometric parameter $G$, calculated by the expression $G = (g_{\|} - 2.0023)/(g_{\perp} - 2.0023)$, is greater than 4 the exchange interaction is negligible, but $G < 4$ indicates considerable exchange interaction in the solid complexes. In the complex (**3**), the $G$ value is about 2.5 indicating exchange interactions in solid complex.

Summarising, in the simple one-pot syntheses isothiocyanate or chloride complexes of manganese(II), nickel(II)

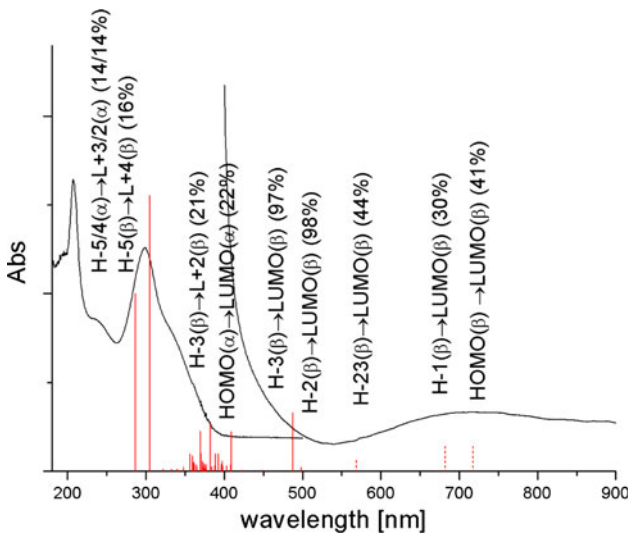


**Fig. 7** The UV–vis spectrum of [Cu(SCN)$_2$(pytriaz)$_2$] (**3**) complexes with calculated transitions

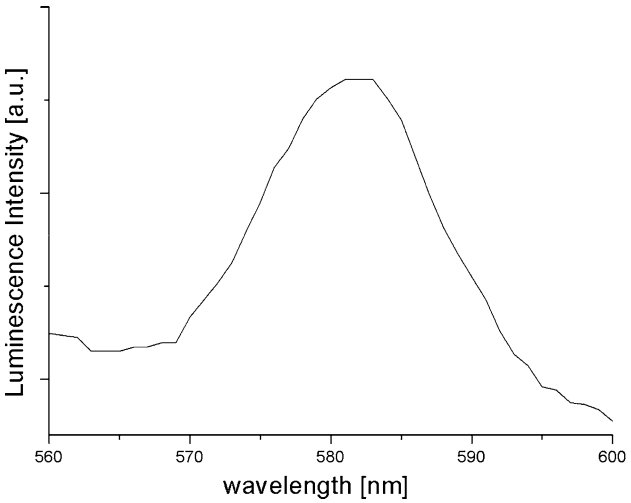


**Fig. 8** The emissions spectrum of the methanolic solution ($c = 5 \times 10^{-4}$ mol/dm$^3$) of complex **2** with excitation at 494 nm

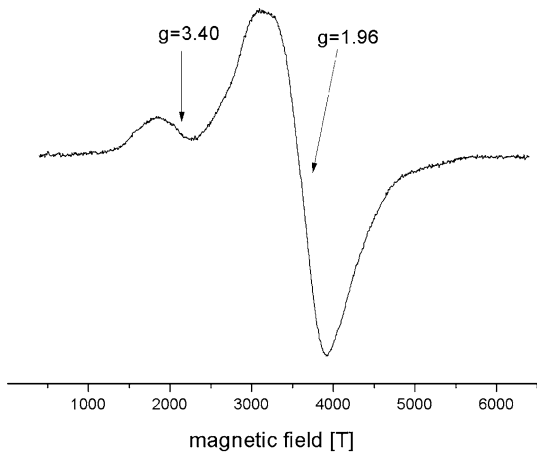


**Fig. 9** The EPR spectra of solid state [Mn(SCN)$_2$(pytriaz)$_2$] (**1**) and [Cu(SCN)$_2$(pytriaz)$_2$] (**3**) complexes

and copper(II) with 5,6-diphenyl-3-(2-pyridyl)-1,2,4-triazine (pytz) and SCN/Cl ligands were obtained. The complexes were characterised by IR, UV–vis, EPR

spectroscopy, and their crystal structures were determined by X-ray diffraction. The experimental studies on the complexes incorporating 5,6-diphenyl-3-(2-pyridyl)-1,2,4-triazine have been accompanied computationally by the density functional theory (DFT) and time-dependent DFT calculations. X-ray studies revealed six-coordinate geometry about the metal centre with two bounded pytz molecules in *trans* bis-chelate configuration in the equatorial plane, and two thiocyanate ions in axial positions. The nickel(II) complex shows a weak luminescent properties. In solid state of copper(II) complex the exchange interactions are expected and the differences between chloride and NCS ligands are demonstrated.

## Supplementary data

CCDC 785978, CCDC 773120 and CCDC 791533 contain the supplementary crystallographic data for complexes [Mn $(SCN)_2(pytz)_2$], $[NiCl_2(pytz)_2]\cdot 2CH_3OH$ and $[Cu(SCN)_2(pytz)_2]$ respectively. These data can be obtained free of charge from http://www.ccdc.cam.ac.uk/conts/retrieving.html, or from the Cambridge Crystallographic Data Centre, 12 Union Road, Cambridge CB2 1EZ, UK; fax: (+44) 1223-336-033; or e-mail: deposit@ccdc.cam.ac.uk Calculations have been carried out in Wroclaw Centre for Networking and Supercomputing (http://www.wcss.wroc.pl).



## References

1. Béreau V, Rey J, Deydier E, Marrot J (2003) Inorg Chim Acta 351:389
2. Béreau V, Marrot J (2005) C. R. Chimie 8:1087
3. Croot PL, Hunter KA (2000) Anal Chim Acta 406:289
4. Almog J, Hirshfeld A, Glattstein B, Sterling J, Goren Z (1996) Anal Chim Acta 322:203
5. Grove H, Julve M, Lloret F, Kruger PE, Törnroos KW, Sletten J (2001) Inorg Chim Acta 325:115
6. Talukder P, Datta A, Mitra S, Rosair G, Fallah MSE, Ribas J (2004) Dalton Trans 4161
7. Youngme S, Phatchimkun J, Suksangpanya U, Pakawatchai Ch, van Albada GA, Quesada M, Reedijk J (2006) Inorg Chem Commun 9:242
8. Mautner FA, Louka FR, LeGuet T, Massoud SS (2009) J Mol Struct 919:196
9. Lu J, Liu H-T, Wang D-Q, Zhang X-X, Li D-Ch, Dou J-M (2009) J Mol Struct 938:299
10. Kong L, Li W-J, Li X-L, Geng W-Q, Hao F-Y, Wua J-Y, Zhou H-P, Yang J-X, Tian Y-P, Jin B-K (2010) Polyhedron 29:1575
11. Carranza J, Sletten J, Lloret F, Julve M (2009) Polyhedron 28:2249
12. Ebralidze II, Leitus G, Shimon LJW, Wang Y, Shaik S, Neumann R (2009) Inorg Chim Acta 362:4713
13. Peters L, Tepedino M-F, Haas T, Hübner E, Zenneck U, Burzlaff N (2009) Inorg Chim Acta 362:2678
14. Frisch MJ, Trucks GW, Schlegel HB, Scuseria GE, Robb MA, Cheeseman JR, Scalmani G, Barone V, Mennucci B, Petersson GA, Nakatsuji H, Caricato M, Li X, Hratchian HP, Izmaylov AF, Bloino J, Zheng G, Sonnenberg JL, Hada M, Ehara M, Toyota K, Fukuda R, Hasegawa J, Ishida M, Nakajima T, Honda Y, Kitao O, Nakai H, Vreven T, Montgomery J A Jr, Peralta JE, Ogliaro F, Bearpark M, Heyd JJ, Brothers E, Kudin KN, Staroverov VN, Kobayashi R, Normand J, Raghavachari K, Rendell A, Burant JC, Iyengar SS, Tomasi J, Cossi M, Rega N, Millam JM, Klene M, Knox JE, Cross JB, Bakken V, Adamo C, Jaramillo J, Gomperts R, Stratmann RE, Yazyev O, Austin AJ, Cammi R, Pomelli C, Ochterski JW, Martin RL, Morokuma K, Zakrzewski VG, Voth GA, Salvador P, Dannenberg JJ, Dapprich S, Daniels AD, Farkas O, Foresman JB, Ortiz JV, Cioslowski J, Fox DJ (2009) Gaussian 09, Revision A.1. Gaussian Inc., Wallingford
15. Becke AD (1993) J Chem Phys 98:5648
16. Lee C, Yang W, Parr RG (1988) Phys. Rev. B 37:785
17. Glendening ED, Reed AE, Carpenter JE, Weinhold F, NBO (version 3.1)
18. O'Boyle NM, Tenderholt AL, Langner KM (2008) J. Comp. Chem. 29:839
19. Tenderholt AL (2007) QMForge, Version 2.1. Stanford University, Stanford
20. Dolomanov OV, Bourhis LJ, Gildea RJ, Howard JAK, Puschmann H (2009) J. Appl. Cryst 42:339
21. Kivelson D, Neiman RR (1961) J Chem Phys 35:149
22. Maki AH, McGarvey BR (1958) J Chem Phys 29:35
23. Wasson JR, Trapp C (1969) J Phys Chem 73:3763
24. Hathaway BJ, Billing DE (1970) Coord Chem Rev 5:143